Supporting Information for:

Preservation of HIV-1 Gag helical bundle symmetry by bevirimat is central to maturation inhibition

Alexander J. Pak[1,⊥], Michael D. Purdy[2], Mark Yeager[2,3,4,5], and Gregory A. Voth[1,6,7,8,#]

[1] Department of Chemistry, The University of Chicago, Chicago, IL 60637
[2] Department of Molecular Physiology and Biological Physics, University of Virginia School of Medicine, Charlottesville, VA 22908
[3] Center for Membrane Biology, University of Virginia School of Medicine, Charlottesville, VA 22908
[4] Cardiovascular Research Center, University of Virginia School of Medicine, Charlottesville, VA 22908
[5] Department of Medicine, Division of Cardiovascular Medicine, University of Virginia School of Medicine, Charlottesville, VA 22908
[6] Chicago Center for Theoretical Chemistry, The University of Chicago, Chicago, IL 60637
[7] Institute for Biophysical Dynamics, The University of Chicago, Chicago, IL 60637
[8] James Franck Institute, The University of Chicago, Chicago, IL 60637

[⊥] Present address: Department of Chemical and Biological Engineering, Colorado School of Mines, Golden, CO 80401

[#]Corresponding author: gavoth@uchicago.edu

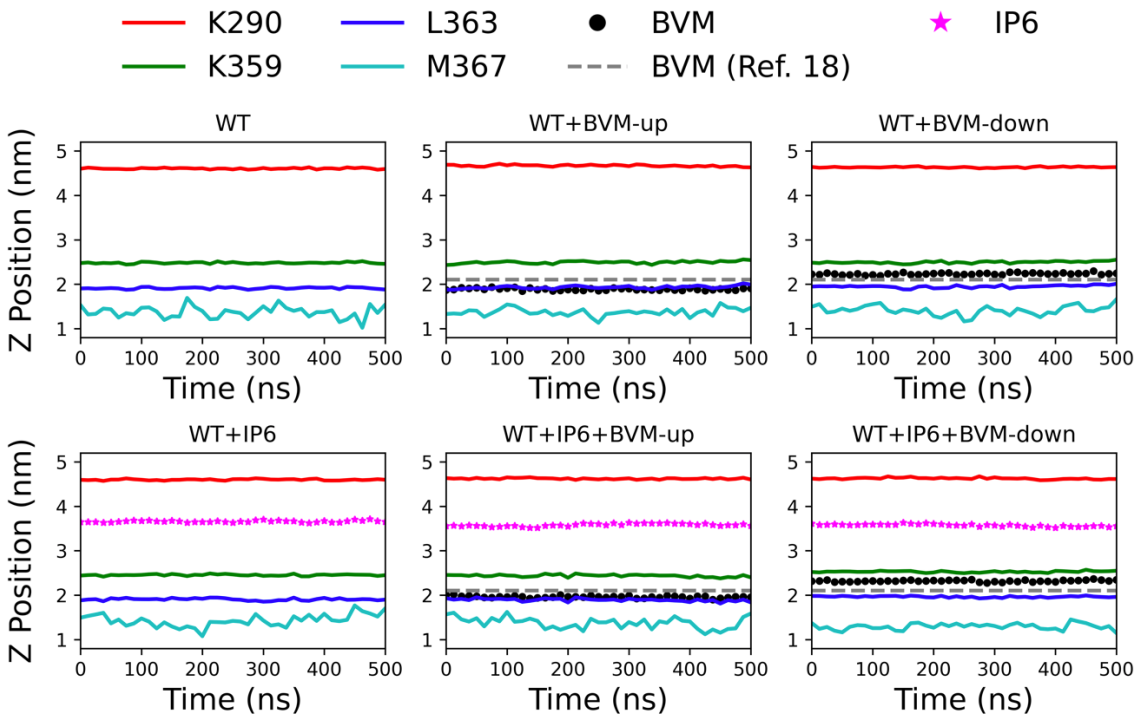

Figure S1. Time-series profiles of the z-position of the centers-of-mass of the BVM pentacyclic triterpenoid moiety, of IP6, and of the C_α within the listed residues throughout the 6HB. Statistics are from the last 500 ns of each trajectory; each line represents the average over 5 replicas. The dashed grey line indicates the position of the BVM pentacyclic triterpenoid moiety from the atomic model resolved in Ref. 18 (of the main text).

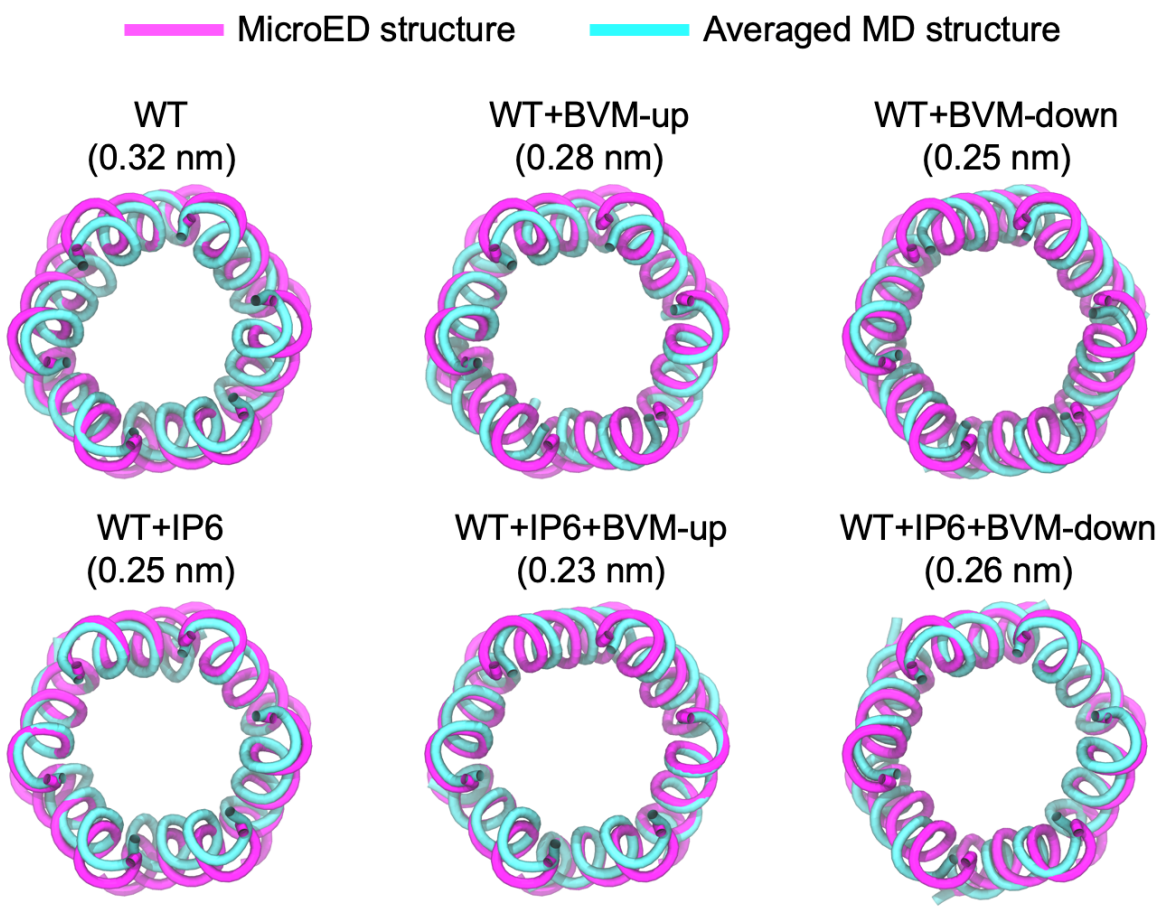

Figure S2. Comparisons between the 6HB structure resolved from MicroED experiments (Ref. 18 of the main text) and the average structure sampled by our MD simulations; each MD structure is averaged over 5 replicas. The root-mean-squared-deviation between the MicroED structure and the structures from MD simulations are presented in parentheses.

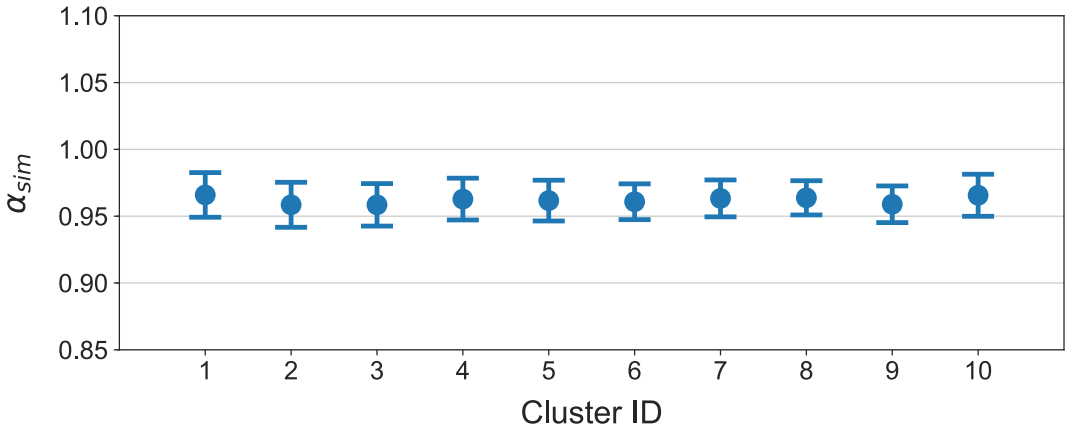

Figure S3. Comparison of α-helix similarity of the Cα backbone (α_{sim}) throughout the six-helical bundle (6HB) for each cluster (see Main Text). The α-helical character in the 6HB is largely preserved and consistent across clusters.

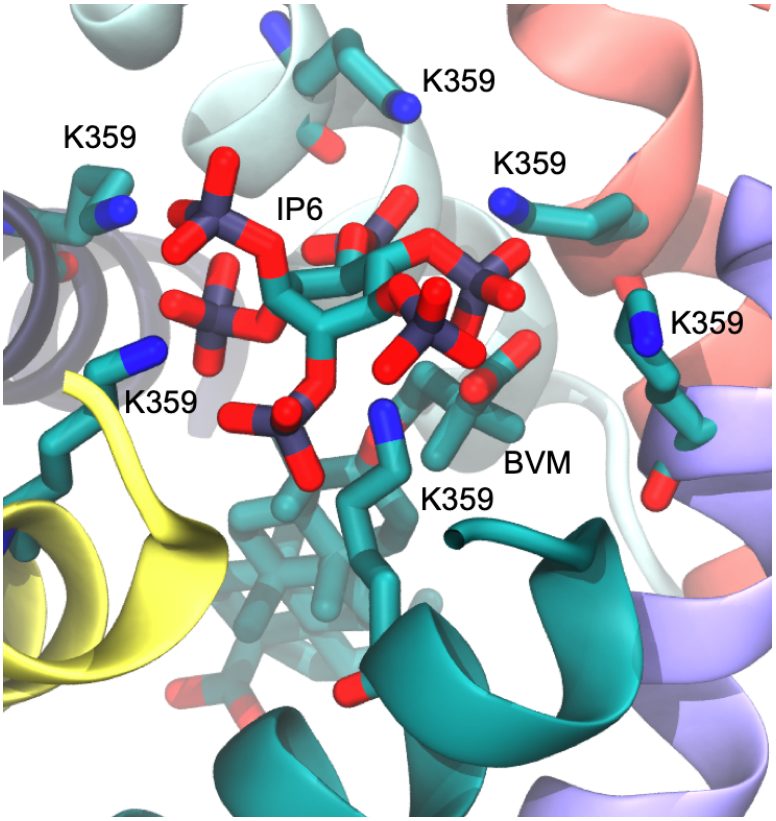

Figure S4. Representative schematic of BVM and IP6 coordinating to K359 within the six-helical bundle. To accommodate coordination between the BVM carboxylic moiety and a lysine sidechain, IP6 tilts yet remains coordinated up to five lysine sidechains.

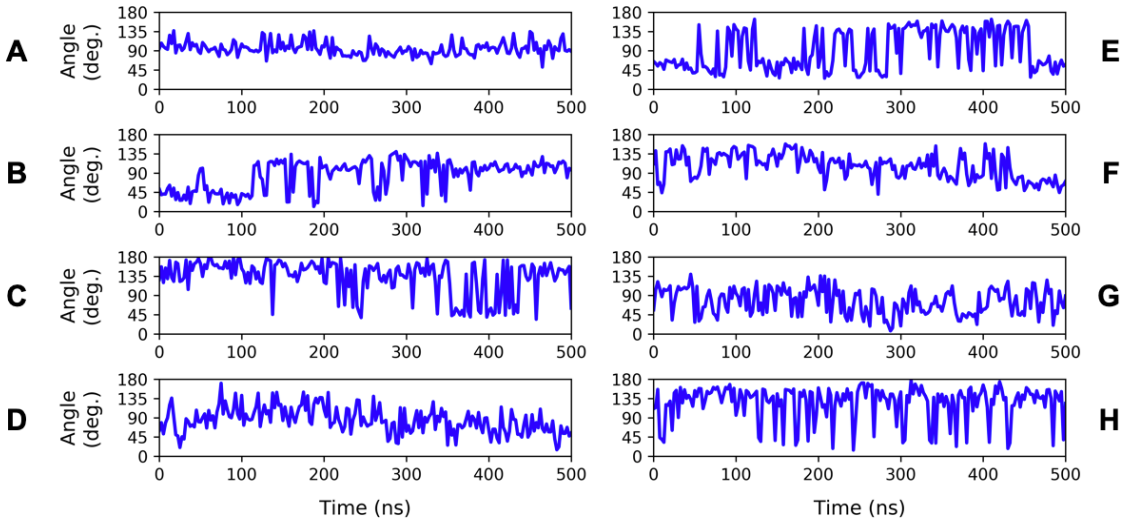

Figure S5. Time series profiles of BVM orientation within the WT 6HB for four different trajectories of (A-D) BVM-up and (E-H) BVM-down. In all cases, the orientation is defined by the angle between the dimethylsuccinyl moiety and the x-axis. IP6 is present in the cases presented in panels C, D, G, and H.

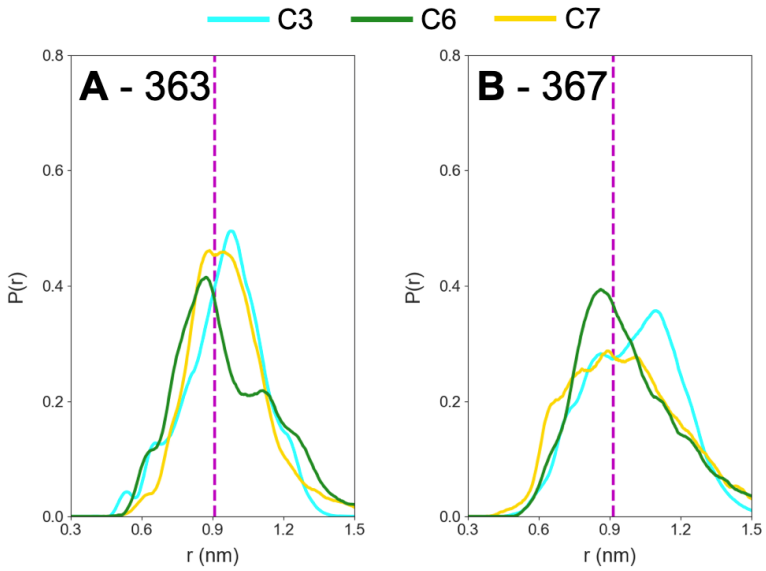

Figure S6. Probability distributions (P(r)) of the radial distance (*r*) between the C atoms in the pentacyclic triterpenoid motif of BVM (see Fig. 4) and C_α atoms of (A) L/F363 and (B) M367 within the listed cluster index (i.e., for clusters 3, 6, and 7). The dashed line indicates the mean *r* between the respective moieties from the atomic model derived by MicroED (Ref. 18).

Table S1. Summary of cluster population statistics from Figure 3.

Virus	C1	C2	C3	C4	C5	C6	C7
	(-) BVM, (-) IP6						
WT	0.00±0.00	0.00±0.00	0.89±0.18	0.00±0.00	0.00±0.00	0.11±0.01	0.00±0.00
L363F	0.02±0.00	0.01±0.00	0.08±0.00	0.89±0.18	0.00±0.00	0.00±0.00	0.00±0.00
A364V	0.00±0.00	0.00±0.00	0.00±0.00	0.44±0.07	0.01±0.00	0.46±0.07	0.09±0.00
V370A	0.00±0.00	0.00±0.00	0.71±0.13	0.02±0.00	0.07±0.00	0.20±0.03	0.00±0.00
	(+) BVM-UP, (-) IP6						
WT	0.44±0.08	0.04±0.00	0.00±0.00	0.22±0.04	0.30±0.06	0.00±0.00	0.00±0.00
L363F	0.00±0.00	0.00±0.00	0.03±0.00	0.17±0.03	0.80±0.18	0.00±0.00	0.00±0.00
A364V	0.00±0.00	0.02±0.00	0.00±0.00	0.21±0.01	0.08±0.00	0.27±0.04	0.42±0.06
V370A	0.00±0.00	0.01±0.00	0.00±0.00	0.15±0.01	0.82±0.15	0.01±0.00	0.01±0.00
	(+) BVM-DOWN, (-) IP6						
WT	0.27±0.03	0.29±0.02	0.00±0.00	0.41±0.06	0.03±0.00	0.00±0.00	0.00±0.00
L363F	0.03±0.00	0.20±0.02	0.00±0.00	0.51±0.08	0.21±0.03	0.01±0.00	0.04±0.01
A364V	0.00±0.00	0.00±0.00	0.00±0.00	0.01±0.00	0.14±0.01	0.25±0.04	0.60±0.13
V370A	0.01±0.00	0.10±0.01	0.00±0.00	0.30±0.03	0.53±0.09	0.04±0.00	0.02±0.00
	(-) BVM, (+) IP6						
WT	0.00±0.00	0.00±0.00	0.96±0.20	0.00±0.00	0.03±0.00	0.01±0.00	0.00±0.00
L363F	0.00±0.00	0.00±0.00	0.12±0.01	0.42±0.07	0.00±0.00	0.46±0.09	0.00±0.00
A364V	0.00±0.00	0.00±0.00	0.06±0.00	0.21±0.02	0.00±0.00	0.73±0.13	0.00±0.00
V370A	0.00±0.00	0.00±0.00	0.84±0.17	0.01±0.00	0.03±0.00	0.01±0.00	0.11±0.01
	(+) BVM-UP, (+) IP6						
WT	0.74±0.15	0.21±0.03	0.00±0.00	0.05±0.00	0.00±0.00	0.00±0.00	0.00±0.00
L363F	0.02±0.00	0.58±0.10	0.00±0.00	0.40±0.06	0.00±0.00	0.00±0.00	0.00±0.00
A364V	0.07±0.00	0.27±0.05	0.00±0.00	0.64±0.12	0.00±0.00	0.02±0.00	0.00±0.00
V370A	0.58±0.09	0.17±0.12	0.00±0.00	0.25±0.02	0.00±0.00	0.00±0.00	0.00±0.00
	(+) BVM-DOWN, (+) IP6						
WT	0.47±0.09	0.35±0.05	0.00±0.00	0.17±0.02	0.00±0.00	0.00±0.00	0.00±0.00
L363F	0.02±0.00	0.30±0.04	0.00±0.00	0.68±0.13	0.00±0.00	0.00±0.00	0.00±0.00
A364V	0.00±0.00	0.00±0.00	0.00±0.00	0.73±0.14	0.15±0.02	0.00±0.00	0.12±0.01
V370A	0.03±0.00	0.40±0.05	0.00±0.00	0.47±0.06	0.10±0.01	0.00±0.00	0.00±0.00